JOURNAL OF MATERIALS SCIENCE 27 (1992) 1061–1069

Mechanism of carburization of high-temperature alloys

H. M. TAWANCY, N. M. ABBAS
Materials Characterization Laboratories, Metrology, Standards and Materials Division, Research Institute, King Fahd University of Petroleum and Minerals, PO Box 1639, Dhahran 31261, Saudi Arabia

An investigation of the mechanism of gaseous carburization in a reducing environment was conducted for selected Fe- and Ni-base alloys. Carburization kinetics were measured as functions of temperature in the range 870–980 °C. Scanning electron microscopy, analytical electron microscopy and X-ray diffractometry were employed for microstructural characterization and microchemical analysis. Changes in mechanical strength produced by carburization were determined from microhardness and tensile property measurements. Kinetic studies indicated that the carburization reaction followed a parabolic rate law. Depending upon the nature of surface scale formed in the presence of a carburizing environment, the rate-determining step of the reaction varied from C diffusion into the alloy in the presence of a carbide scale to that in the presence of an oxide scale. Under reducing carburizing conditions, alloys inherently protected by Cr_2O_3-base scale were found to develop a surface carbide scale which allowed C to penetrate into the alloy with relative ease and, thus, the carburization kinetics was accelerated. In contrast, an alloy capable of forming Al_2O_3 developed and maintained a protective surface oxide scale which acted as an effective barrier to C diffusion into the alloy. Degradation of mechanical strength due to precipitation of carbides in the alloy was correlated with the rate of attack and consequently the nature of the surface scale.

1. Introduction

Carburization attack is an important mode of high-temperature corrosion, particularly at temperatures in excess of about 900 °C (e.g. [1, 2]). It is encountered in many petrochemical industrial processes such as ethylene cracking and methanol production [3]. Examples of components which can become subject to a carburization attack include heat exchangers, pyrolysis tubes and pigtails. Typically, in the above processes, the environment is reducing and characterized by a low oxygen potential and high carbon activity ($a_c \simeq 1$) [4–6]. Iron-base alloys and stainless steels are commonly used as structural materials in applications involving high-temperature carburization attack. However, some of the Ni-base alloys can also be suitable for these applications [4, 5].

During a carburization attack, C is generated by reactions involving carbonaceous gases such as CH_4 and CO. It is generally agreed that carburization of Fe-base alloys is controlled by C diffusion into the alloy through a layer of carbide scale which may contain an oxide phase, depending on the alloy composition and whether the environment is reducing or oxidizing [6–10]. Also, the solubility of C in the alloy which is a function of chemical composition can play an important role in carburization [6]. Reaction of C with carbide-forming elements, particularly Cr, leads in the latter case to precipitation of various Cr-rich carbide phases. At the metal surface where the C activity is relatively high, the carbide phase can be of the form M_3C_2. However, as the C activity decreases with increasing distance from the surface, the nature of the carbide phase may change to M_7C_3- and $M_{23}C_6$-type [1, 4–6, 11]. Massive precipitation of Cr-rich carbides in the alloy can result in degradation of (i) ductility and (ii) chemical stability due to localized depletion in Cr.

Formation of surface oxide scale which impedes C diffusion into the alloy can be most effective in reducing or preventing carburization attack [6, 12–15]. Impedance of C diffusion is expected to be dependent upon (i) the nature of surface oxide scale which the alloy can inherently develop, and (ii) the oxygen potential of the environment. Under reducing conditions, Cr_2O_3-forming alloys may not be capable of maintaining a protective surface scale because of the lower thermodynamic stability of Cr_2O_3 in comparison with a carbide scale [4, 5]. More stable oxide scales such as Al_2O_3 can, however, be maintained even under reducing conditions provided the alloy contains a sufficient concentration of Al [4–6, 16].

To further clarify the mechanism of carburization in Fe- and Ni-base alloys, the present investigation was undertaken with emphasis on (i) microstructural changes and microchemical inhomogeneities created by the carburization attack, (ii) the nature of the

surface scale and its influence on the carburization resistance, and (iii) the corresponding effects on mechanical strength.

2. Experimental procedure

Three solid-solution strengthened wrought alloys of commercial grade were selected for this investigation. They included 310ss, Haynes alloy no. 556 and Haynes alloy no. 214 (Haynes is a registered trademark of Haynes International). Table I summarizes their nominal chemical compositions. Both of the Fe-base alloys (556 and 310ss) are inherently protected by Cr_2O_3-base scale. However, the Ni-base alloy 214 is capable of developing Al_2O_3-base scale. Sheet specimens were exposed to a reducing carburizing environment consisting of Ar–5% H_2–5% CO–5% CO_2 by volume [4, 5]. Such an environment is characterized by a high carbon activity ($a_c \simeq 1$) and a low oxygen potential. Exposure times varied from 24 to 215 h at temperatures in the range 870 to 980 °C. Under these conditions, the kinetics of the carburization reaction was found to follow a parabolic rate law similar to other alloys [6–10]. From weight-change measurements as a function of exposure time at a given temperature, the temperature-dependent reaction rate constant (K) was calculated from $(\Delta W)^2 = Kt$ where ΔW is the specimen weight change and t is the exposure time at a given temperature [17, 18].

Conventional scanning electron microscopy (SEM) and the transmission electron microscopy (TEM) and SEM modes of an analytical electron microscope operating at 200 kV were employed for microstructural characterization. Thin foils for TEM were prepared by the jet-polishing technique in a solution consisting of 30% nitric acid in methanol at about − 20 °C. Energy-dispersive X-ray spectroscopy (EDXS) using an ultra-thin window detector capable of detecting C was utilized for microchemical analysis. Phase analysis of surface scale was conducted in an X-ray diffractometer.

Changes in mechanical properties associated with carburization were determined from microhardness measurements and room-temperature tensile tests. To determine the effect of carburization on tensile ductility, one set of tensile specimens (50.8 mm gauge length) from each alloy was exposed 24 h at 980 °C in the carburizing environment and another set was exposed 24 h at 980 °C in air prior to testing. Fractography was conducted in a conventional SEM.

TABLE I Nominal chemical compositions of the alloys investigated

Element	Alloy composition (wt %)		
	310ss	556	214
Ni	20	20	Balance
Fe	Balance	Balance	
Cr	25	22	16
Mo	–	3	–
W	–	2.5	–
Mn	2[a]	1	–
Si	1.5[a]	0.4	–
C	0.25[a]	0.1	0.04
Others	–	0.2Al	4.5Al
		0.8 (Nb + Ta)	0.01Y
		0.02La	
		0.2N	
		0.02Zr	

[a] Maximum.

3. Results and discussion

3.1. Carburization kinetics

Fig. 1 illustrates the functional dependence of the reaction rate constant (K) on temperature for each of the alloys investigated. It is observed that the carburization kinetics follows a parabolic rate law similar to other alloys [6–9]. From the data of Fig. 1, the alloys investigated can be ranked in order of increasing carburization kinetics as: alloy 214, alloy 556 and 310ss. Table II summarizes the activation energy of carburization for each of the three alloys as calculated from the slopes of the lines in Fig. 1.

Activation energies of 130 and 170 kJ mol^{-1} for 310ss and alloy 556, respectively, appeared to be consistent with a carburization reaction controlled by C diffusion into the alloy in the presence of a less protective surface carbide scale and the absence of a more protective oxide scale [6–9]. It is possible that the rapid carburization kinetics of 310ss in comparison with alloy 556 is related to differences in the solubility and diffusivity of C [6]. Solubility of C in the alloy is expected to be a function of alloy chemistry. Among the elements believed to influence the C solubility is Ni [19, 20]. Assuming that Co behaves similarly to Ni, the greater (Ni + Co) content of alloy 556 (Table I) may explain, at least partially, the slower

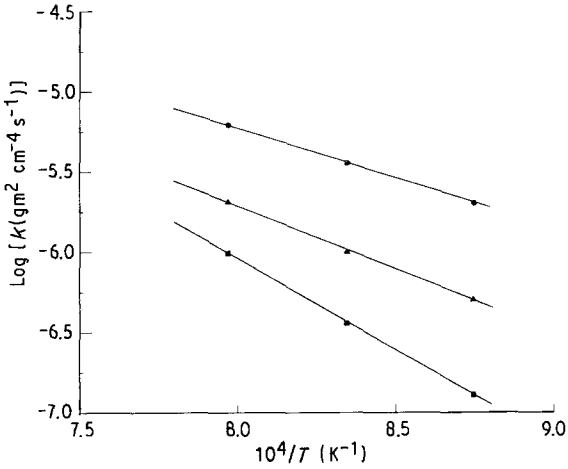

Figure 1 Functional dependence of the parabolic carburization rate constant (K) on temperature for each of the alloys investigated: (●) 310ss, (▲) alloy 556, (■) alloy 214.

TABLE II Activation energies of the carburization reaction

Alloy	Activation energy (kJ mol^{-1})
310ss	130
556	170
214	235

kinetics in the case of alloy 556. Also, Ni is believed to reduce the C diffusivity in the alloy [21].

For the Fe-base alloy 800H (Fe–33Ni–21Cr) which is commonly used in applications involving a carburization attack, the activation energy in a reducing environment was reported to be 178 kJ mol^{-1} [6] and 167 kJ mol^{-1} [9]. Both values approach the activation energy for alloy 556 (170 kJ mol^{-1}). It is interesting to note that when the results of carburization tests are expressed in terms of mass of C pick-up per unit area, both alloys 800H and 556 exhibit similar resistances to carburization over the temperature range 870 to 980 °C [4, 5]. Another interesting feature of the two alloys is that the Ni content of alloy 800H (33 wt %) approaches the (Ni + Co) content of alloy 556 (38 wt %). Thus, it is possible that for certain alloys, a correlation may exist between the kinetics of carburization and the (Ni + Co) content.

When only Cr and Fe are the major carbide-forming elements in the alloy as in the case of 310ss, alloy 800H and alloy 556, it is found that a correlation exists between the resistance to carburization in a reducing environment and the Ni/(Cr + Fe) ratio [8]. An improvement in carburization resistance by a factor of three was observed when this ratio was increased from 0.3 to 1.0 [8]. If instead, the above ratio is expressed as (Ni + Co)/(Cr + Fe), its value becomes 0.26, 0.52 and 0.71 for alloys 310ss, 800 H and 556, respectively. Thus it would be expected that the carburization resistance of 310ss is considerably lower than that of alloys 800H and 556. However, it is important to point out that when other elements which can significantly influence the carburization behaviour are present in significant concentrations, e.g. Mo, W, Ti, Al and Si, the above correlation may no longer be valid [4, 5]. Also, it is likely that the above correlation holds only in a reducing environment where a protective Cr_2O_3-base scale cannot be maintained. Consequently, reducing the Cr content in this case can be beneficial because it decreases the density of carbide precipitates in the alloy. In contrast, the presence of a high Cr content is expected to have a beneficial effect in an oxidizing environment where a protective Cr_2O_3-base scale can be maintained.

Unlike the case described above for 310ss and alloy 556, the greater activation energy of 235 kJ mol^{-1} for alloy 214 suggested that carburization occurred in the presence of a protective oxide scale [6, 9], which was identified to be based on Al_2O_3 as shown below. It is noted that the activation energy for alloy 214 is comparable to that of 220 kJ mol^{-1} reported for an Ni-base alloy containing 3.31 wt % Si and tested in a reducing carburizing environment [9]. Also, high activation energies were reported for Fe-base alloys containing significant concentrations of Al, Si or Ti [6]. Like Al in alloy 214, Si and Ti can be expected to promote the formation of a protective oxide scale.

Microstructural characterization confirmed the above suggestions concerning the relationship between carburization kinetics and nature of surface scale for the alloys investigated as described below.

TABLE III X-Ray diffractometer data illustrating the identification of Cr_3C_2 surface scale on a specimen of 310ss after carburization testing at 980 °C (orthorhombic: $a = 0.552$, $b = 1.149$ and $c = 0.283$ nm)

$d_{calc.}$ (nm)	$d_{obs.}$ (nm)	($h k l$)
0.275	0.273	(0 1 1)
0.256	0.255	(1 4 0)
0.249	0.247	(2 2 0)
0.246	0.243	(1 1 1)
0.230	0.229	(1 2 1)
0.227	0.225	(0 3 1)
0.224	0.223	(2 3 0)
0.212	0.211	(1 5 0)
0.210	0.208	(1 3 1)
0.199	0.198	(2 4 0)
0.195	0.194	(2 1 1)

3.2. Microstructural characterization

Analysis of the surface scale formed on the Cr_2O_3-forming alloys (310ss and 556) by X-ray diffraction revealed the absence of surface oxide scale. Instead, the scale was found to predominantly consist of a phase isomorphous with Cr_3C_2 as exemplified in Table III for 310ss.

Qualitatively, both 310ss and alloy 556 exhibited a similar attack morphology. An example derived from 310ss after 215 h exposure at 925 °C is given in Fig. 2. As can be seen from Fig. 2a, the morphology of attack is characterized by the presence of a layer of surface scale followed by a precipitate-free zone and then a region of high precipitate density. Similar to the results of X-ray diffraction (Table III), microchemical analysis by EDXS showed that the surface scale consisted mostly of a Cr-rich carbide (dark phase marked 1 in Fig. 2a) as illustrated in the X-ray spectrum of Fig. 2b. In addition to Cr, the carbide can be seen to contain a significant concentration of Fe and a very small concentration of Ni. This observation reflects the tendency of both Cr and Fe to form stable carbides and the thermodynamic instability of Ni carbides. Beneath the carbide scale a small proportion of an oxide phase enriched in Cr and Fe was detected (bright phase marked 2 in Fig. 2a). A corresponding X-ray spectrum is shown in Fig. 2c. As might be expected, the oxide phase is of the form $(Cr, Fe)_2O_3$. It is clear from Fig. 2a that during the progress of the carburization reaction, the carbide scale had overgrown the oxide scale. Fig. 2d illustrates the results of point analysis of the Cr content across the line xx in Fig. 2a. Within the carbide scale, a high Cr concentration is observed as expected. However, a considerable depletion of Cr is observed in the precipitate-free zone underneath the scale. Evidently, depletion of Cr near the surface due to the formation of surface carbide scale reduced the ability of the alloy to form a more protective oxide scale. Consequently, the carbide scale had overgrown the oxide scale as observed (Fig. 2a). With increasing distance from the surface, the Cr concentration can be seen to reach the level typical of the alloy.

In the early stages of exposure of both 310ss and alloy 556, e.g. 24 h at a given temperature, a relatively

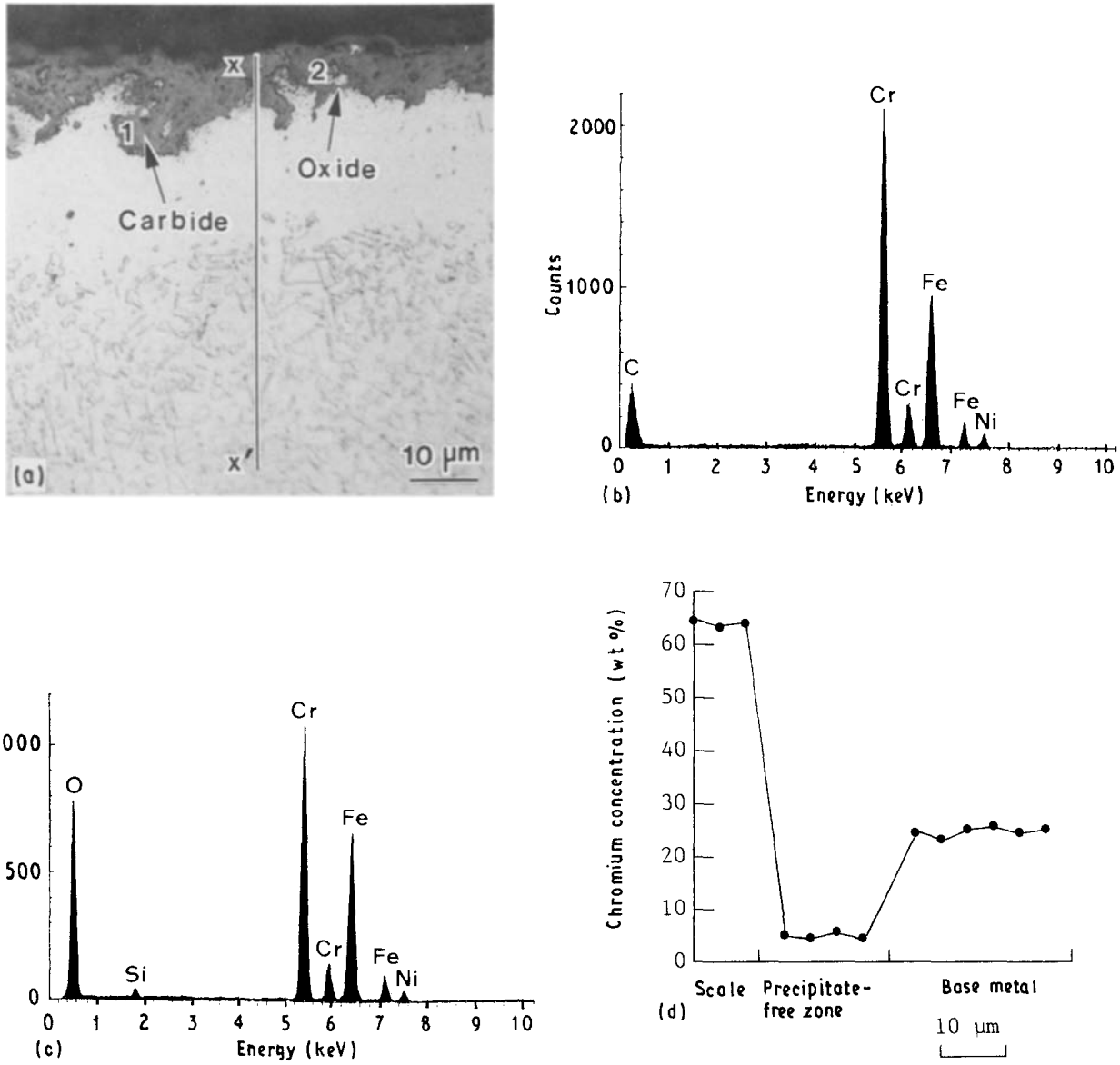

Figure 2 Analysis of the scale components formed on 310ss after 215 h exposure at 925 °C in the carburizing environment. (a) Conventional backscattered electron composition image illustrating the morphological features of the surface scale and alloy substrate. (b) X-ray spectrum derived from the region marked (1) in (a). (c) X-ray spectrum derived from the region marked (2) in (a). (d) Analysis of the Cr concentration along xx′ in (a).

small density of M_7C_3-type carbide (hexagonal, $a = 1.396$; $c = 0.451$ nm) was detected in thin foils prepared from sections near the surface as illustrated in the example of Fig. 3. A distinguishing feature of this carbide is its internal structure which consists of fine striations (Fig. 3a and c) due to the presence of stacking faults on the basal plane and planes normal to it [22]. Diffraction streaks can be seen along $\langle 10\bar{1}0 \rangle$ and $\langle 01\bar{1}0 \rangle$ directions in the corresponding selected-area diffraction pattern of Fig. 3b, which indicates the presence of faults on planes normal to the basal plane. Due to the complexity of the crystal structure of M_7C_3-type carbide, it is rather difficult to correlate the presence or absence of certain reflections with the results of structure factor calculations [22]. A typical X-ray spectrum derived from the carbide particle of Fig. 3a is shown in Fig. 3d. As with M_3C_2-type carbide (Fig. 2b), it can be seen that the M_7C_3-type carbide contains a relatively high concentration of Fe and a very small concentration of Ni. After extended exposure at a given temperature, however, M_7C_3-type carbide was rarely observed. This is consistent with the tendency of this carbide to transform into the more stable $M_{23}C_6$-type carbide with continued exposure at a given temperature [23].

Most of the matrix and grain-boundary precipitates observed in Fig. 2a were identified by electron diffraction and EDXS to be the Cr-rich $M_{23}C_6$ (fcc, $a = 1.085$ nm). An example derived from alloy 556 is given in Fig. 4. Generally, the density of $M_{23}C_6$ carbide in alloy 556 was smaller than that in 310ss. Fig. 5 illustrates the result of a dark-field TEM experiment for identification of $M_{23}C_6$ carbide precipitates at a grain boundary in a specimen of 310ss.

Massive carbide precipitates in the matrices of 310ss and alloy 556 such as those shown in Figs 2a and 3a, respectively, suggested that the carbide scale permitted C to penetrate into the alloy with relative ease. It is to be noted that the atomic mobility within Cr_3C_2 is rather high due to its small binding energy as reflected by its enthalpy of formation [24]. As a result, the carburization kinetics was accelerated.

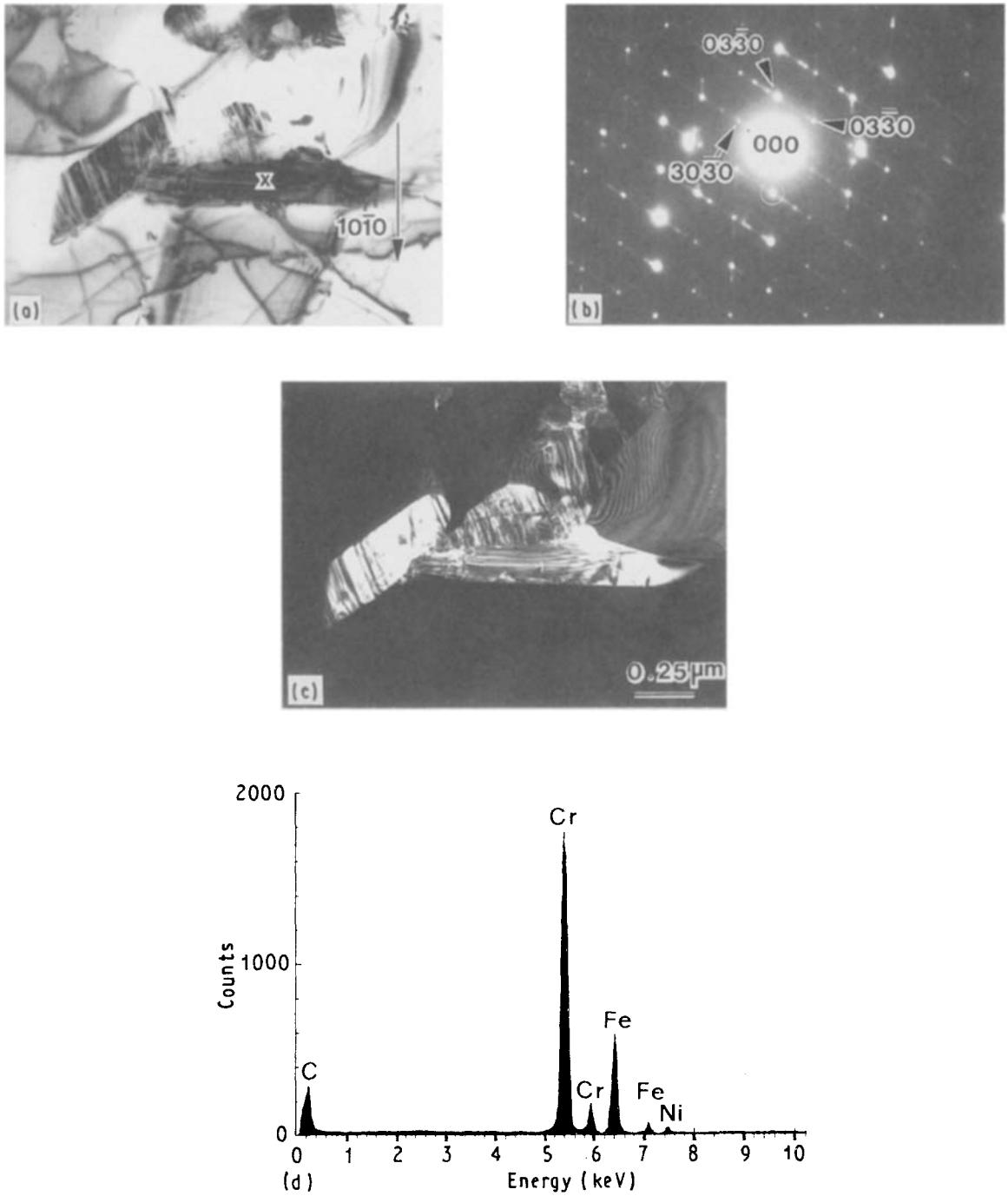

Figure 3 Identification of M_7C_3-type carbide in alloy 556 after 24 h exposure at 925 °C in the carburizing environment. (a) Bright-field TEM image illustrating characteristic fine striations within a carbide particles due to the presence of stacking faults. (b) Corresponding SAD pattern near (0 0 0 1) orientation. Streaking due to stacking faults is observed along $\langle 10\bar{1}0 \rangle$ and $\langle 01\bar{1}0 \rangle$. (c) Dark-field image formed with the encircled reflection in (b). (d) X-ray spectrum derived from the region marked (×) within the carbide particle in (a).

In contrast to the case of 310ss and alloy 556 described above, alloy 214 was found to develop an Al-rich surface oxide scale even under the conditions of a reducing carburizing environment. Fig. 6a is an example illustrating EDXS analysis of the surface scale formed on alloy 214 after 215 h exposure at 925 °C. It is observed that the scale contains a moderate concentration of Cr and a very small concentration of Ni. These data suggested that the oxide scale was essentially of the form $(Al, Cr)_2O_3$. It is to be noted that the thermodynamic stability of Al_2O_3 is considerably higher than that of Cr_2O_3 [24]. Thus, it is possible that Al_2O_3 could form even under reducing conditions. Also, the atomic mobility within Al_2O_3 is expected to be very slow because of its high binding energy [24]. Due to the above characteristics, Al_2O_3-base scale can be expected to act as an effective barrier to C diffusion into the alloy in a carburizing environment. Therefore, both the carburization kinetics and the density of carbide precipitates in the alloy are considerably reduced. For example, a typical microstructure of the alloy after 215 h exposure at 925 °C in the carburizing environment is shown in Fig. 6b. In comparison with 310ss and alloy 556, the density of $M_{23}C_6$ carbide precipitates can be seen to be considerably smaller. It could thus be concluded that

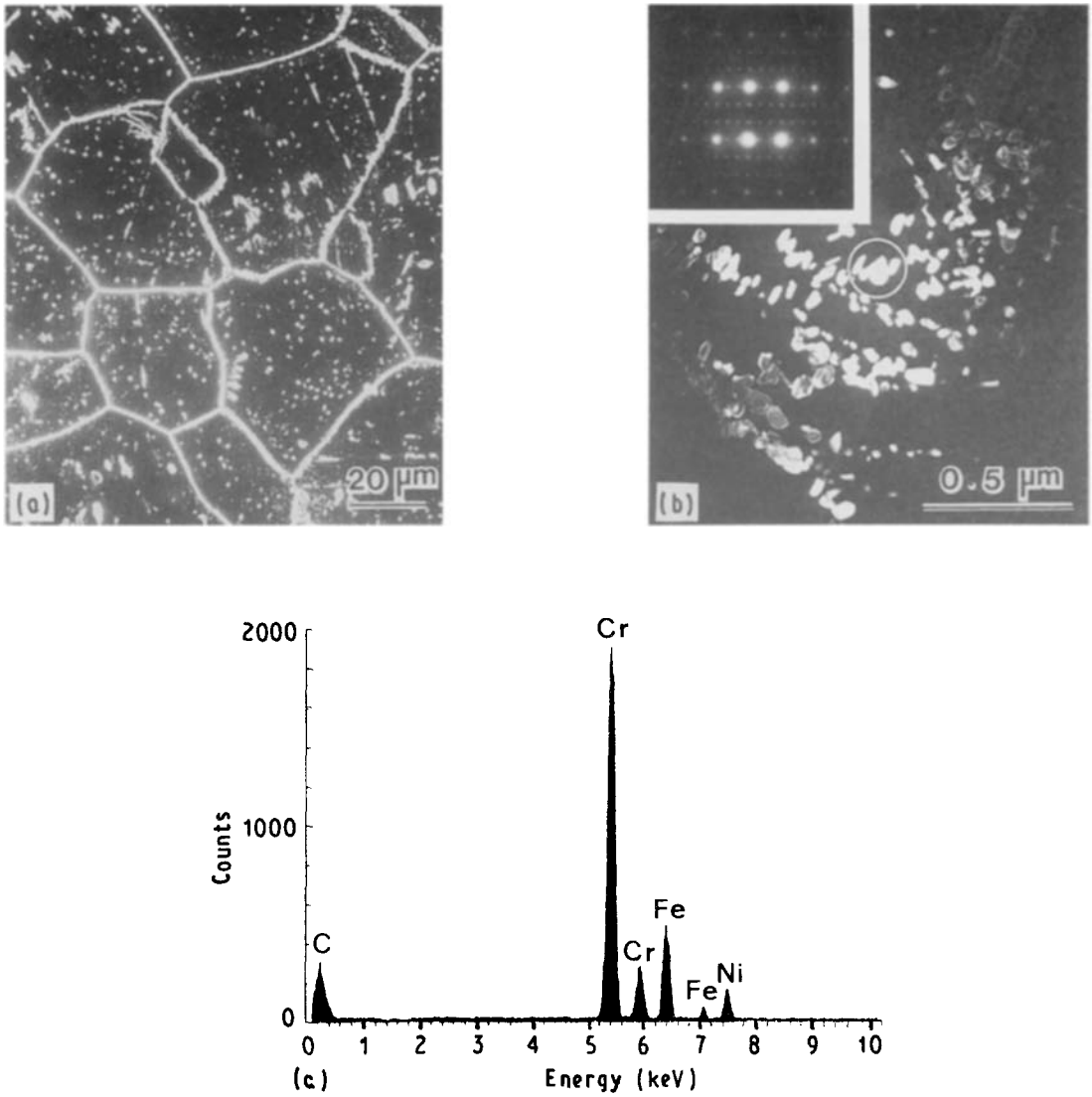

Figure 4 An example illustrating $M_{23}C_6$-type carbide precipitates in the matrix and at grain boundaries of alloy 556 after 215 h exposure at 925 °C in the carburizing environment. (a) Secondary-electron SEM image derived from a thick section of a thin-foil specimen at 200 kV. It illustrates matrix and grain-boundary precipitates. (b) Dark-field TEM image formed with an $M_{23}C_6$ reflection to illustrate $M_{23}C_6$ carbide particles in the matrix. The inset is a microdiffraction pattern derived from the encircled carbide particle in ⟨1 1 2⟩ orientation. (c) X-ray spectrum derived from the encircled particle in (b).

alloys inherently protected by Al_2O_3-base scale offer a substantially greater resistance to carburization in comparison with Cr_2O_3-forming alloys.

3.3. Effect of carburization on mechanical strength

As pointed out earlier, carburization can have an adverse effect on ductility. Over the temperature range investigated, the carburization attack was most severe at 980 °C. For example, Fig. 7 illustrates the result of microhardness measurement as a function of distance from the surface of a 310ss specimen after 24 h exposure at 980 °C in the carburizing environment. It is observed that a considerably hardened surface layer about 50 μm thick was created as a result of the carbon pick-up. Fig. 8 illustrates the effect of carburization on the room-temperature tensile ductilities of the alloys investigated. Although both 310ss and alloy 556 suffered a severe loss of ductility, alloy 214 maintained a high ductility level. This observation is consistent with the effectiveness of Al_2O_3-base scale in resisting carburization attack and its adverse effect on ductility.

Both 310ss and alloy 556 exhibited an intergranular fracture mode after carburization. An example illustrating the effect of carburization on the tensile fracture behaviour of 310ss is given in Fig. 9. Extensive intergranular cracking is observed near the surface of a tensile-tested specimen as illustrated in Fig. 9a, which is consistent with the presence of a considerably hardened surface layer (Fig. 7). As can be concluded from Fig. 9b, the tensile fracture mode was predominantly intergranular.

3.4. Carburization mechanism

To describe the mechanism of carburization in a reducing environment, the behaviour of two groups of alloys must be distinguished: first, alloys which are incapable of developing a protective oxide scale and secondly, alloys which can develop and maintain a protective oxide scale. Based on the results presented above, it is possible to describe the mechanism of carburization in each case as follows:

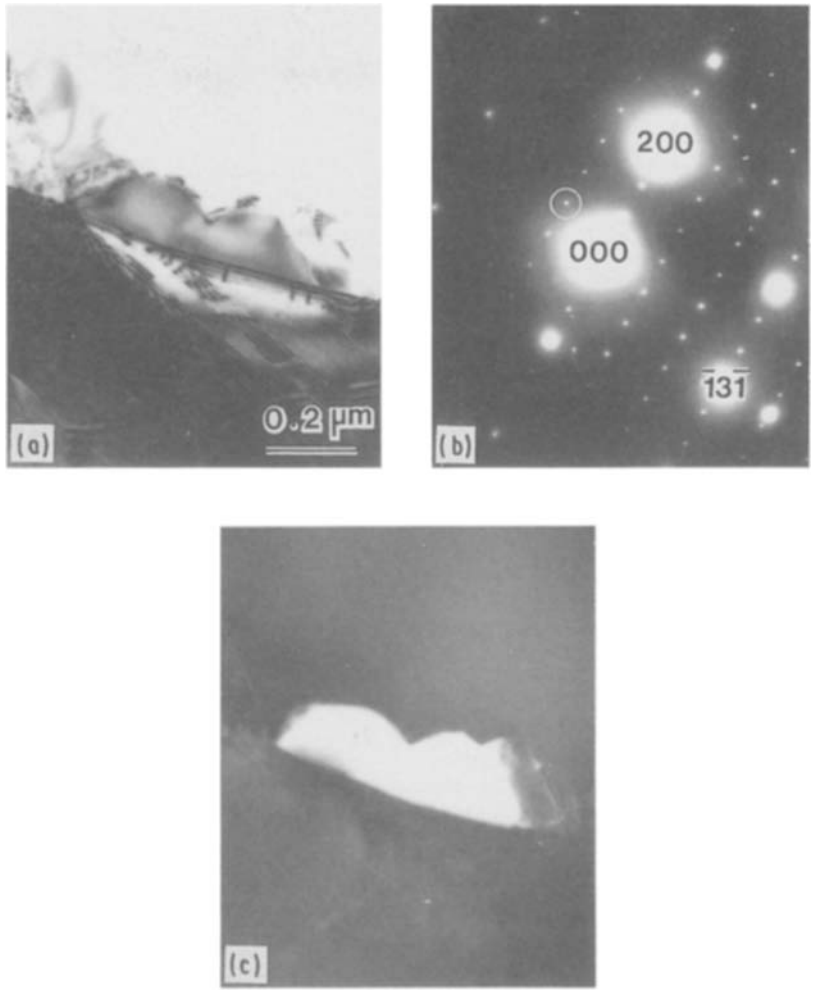

Figure 5 Identification of $M_{23}C_6$ carbide precipitate at a grain boundary of 310ss after 215 h exposure at 925 °C in the carburizing environment. (a) Bright-field TEM image. (b) Corresponding SAD pattern near ⟨0 1 3⟩ orientation, illustrating characteristic reflections of $M_{23}C_6$ carbide at 1/3 positions of the matrix reflections. (c) Dark-field TEM image formed with the encircled reflection in (b).

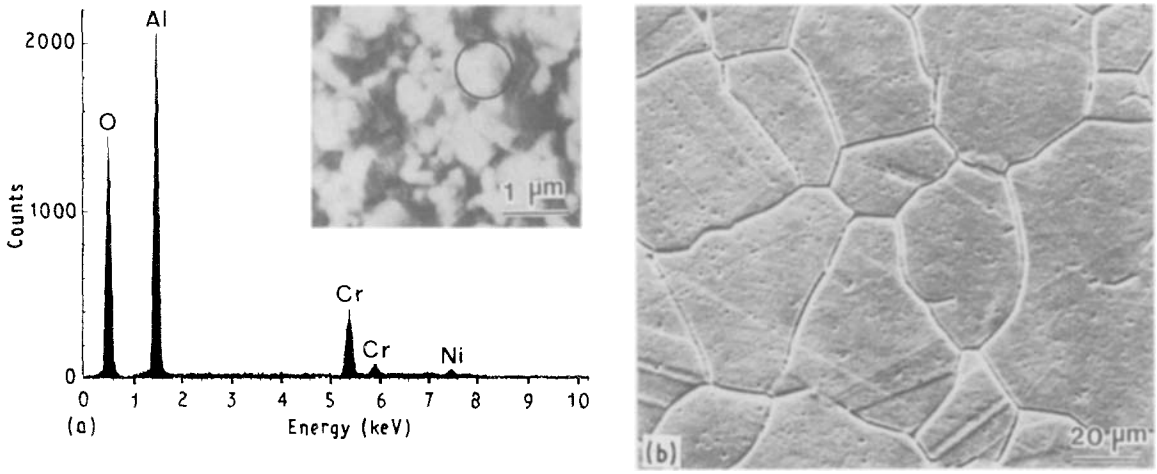

Figure 6 Analysis of surface scale formed on alloy 214 and microstructure of alloy substrate after 215 h exposure at 925 °C in the carburizing environment. (a) X-ray spectrum derived from the encircled region in the secondary-electron SEM image of the inset. (b) Conventional secondary-electron SEM image illustrating a very small density of fine carbide precipitates in the alloy substrate.

During heating to the reaction temperature of alloys inherently protected by Cr_2O_3, it is possible that an oxide phase initially forms. It is noted that oxidation can occur at lower temperatures even under conditions of low oxygen potential [9]. Carbon generated by reactions involving carbonaceous gases reacts with Cr at the alloy surface to form a carbide scale of the M_3C_2 type if the C activity at the surface is sufficiently high, as in the present case. Subsequently, the more stable carbide phase overgrows the oxide

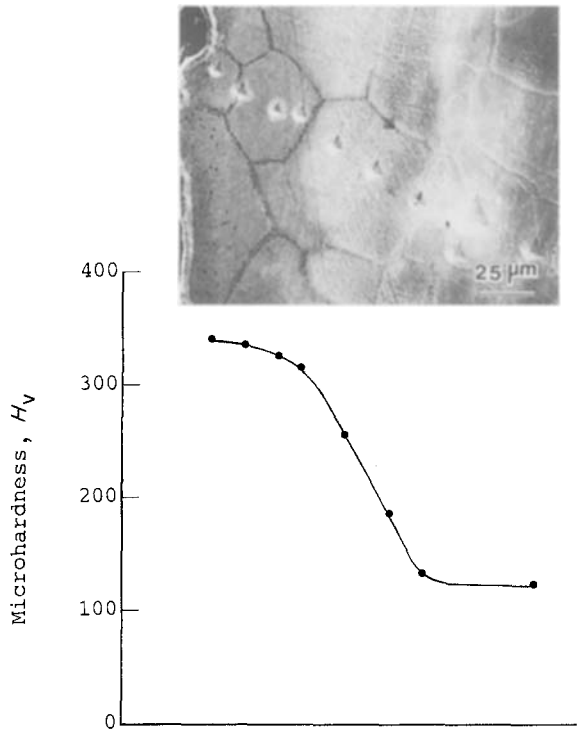

Figure 7 An example demonstrating the hardening produced by carburization of 310ss (specimen exposed 24 h at 980 °C). The micrograph illustrates the regions from which the microhardness data was derived.

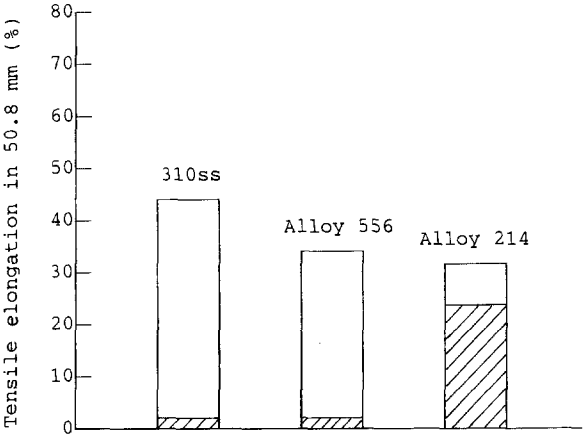

Figure 8 Effect of 24 h exposure at 980 °C in air (unshaded) and in the carburizing environment (shaded) on the room-temperature tensile ductilities of the alloys investigated.

phase as schematically illustrated in Fig. 10a, which is consistent with the observation of Fig. 2a. Depletion of Cr in the alloy substrate due to continued growth of the surface carbide scale precludes the formation of a more protective oxide scale. Due to the relatively high atomic mobility within the carbide scale, C can penetrate into the alloy with relative ease and results in massive precipitation of carbide phases which degrade the mechanical strength of the alloy.

Alloys inherently protected by Al_2O_3 can develop and maintain a protective oxide scale even under reducing conditions, as schematically illustrated in Fig. 10b. An example of this behaviour has been given in Fig. 6. In the early stages of the reaction and prior

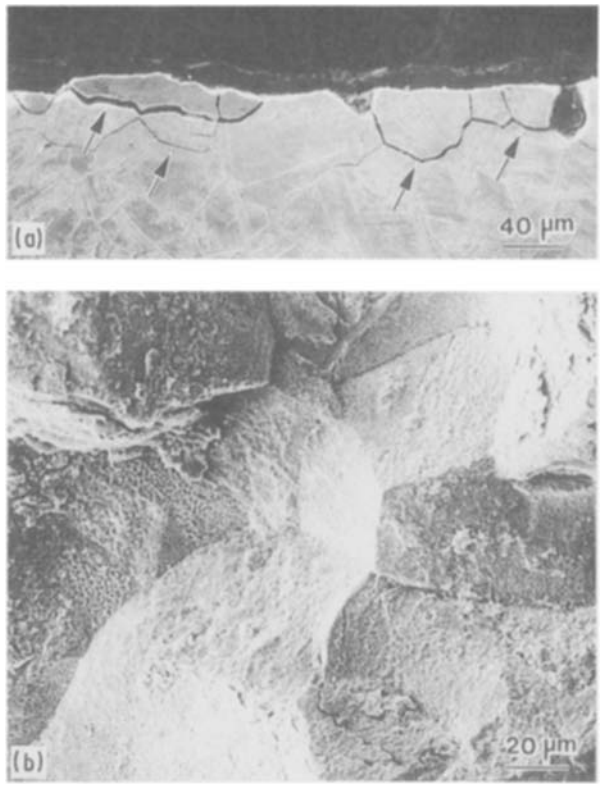

Figure 9 Secondary-electron SEM images illustrating the effect of carburization on the tensile fracture behaviour of 310ss (specimen exposed 24 h at 980 °C in the carburizing environment and then tensile-tested at room temperature). (a) Image of the specimen surface, illustrating extensive intergranular cracking as indicated by the arrows. (b) Fractograph illustrating a predominant intergranular fracture mode.

to developing a continuous oxide scale, some C can penetrate into the alloy and this results in precipitation of a small density of carbides. Subsequently, a continuous protective scale is developed which acts as an effective barrier toward C diffusion into the alloy. As a result, massive precipitation of carbide phases is prevented. Thus, an alloy protected by Al_2O_3-base scale is expected to be highly resistant to a carburizing environment, as experimentally observed.

4. Conclusions

The carburization kinetics of selected Fe- and Ni-base alloys exposed to a reducing environment was found to follow a parabolic rate law. Diffusion of C into the alloy was found to be the rate-determining step of the reaction. Alloys inherently protected by Cr_2O_3-base scale appeared to be incapable of developing a protective surface oxide scale under reducing conditions. Consequently, these alloys experienced a greater rate of attack in comparison with alloys capable of developing the more stable Al_2O_3-base scale. A correlation was found between the rate of carburization and loss of tensile ductility. Alloys incapable of developing a protective oxide scale suffered a considerable loss of ductility, which led to extensive intergranular embrittlement. In the presence of a protective Al_2O_3-base scale, however, a moderate ductility loss was experienced. A highly stable oxide scale such as Al_2O_3

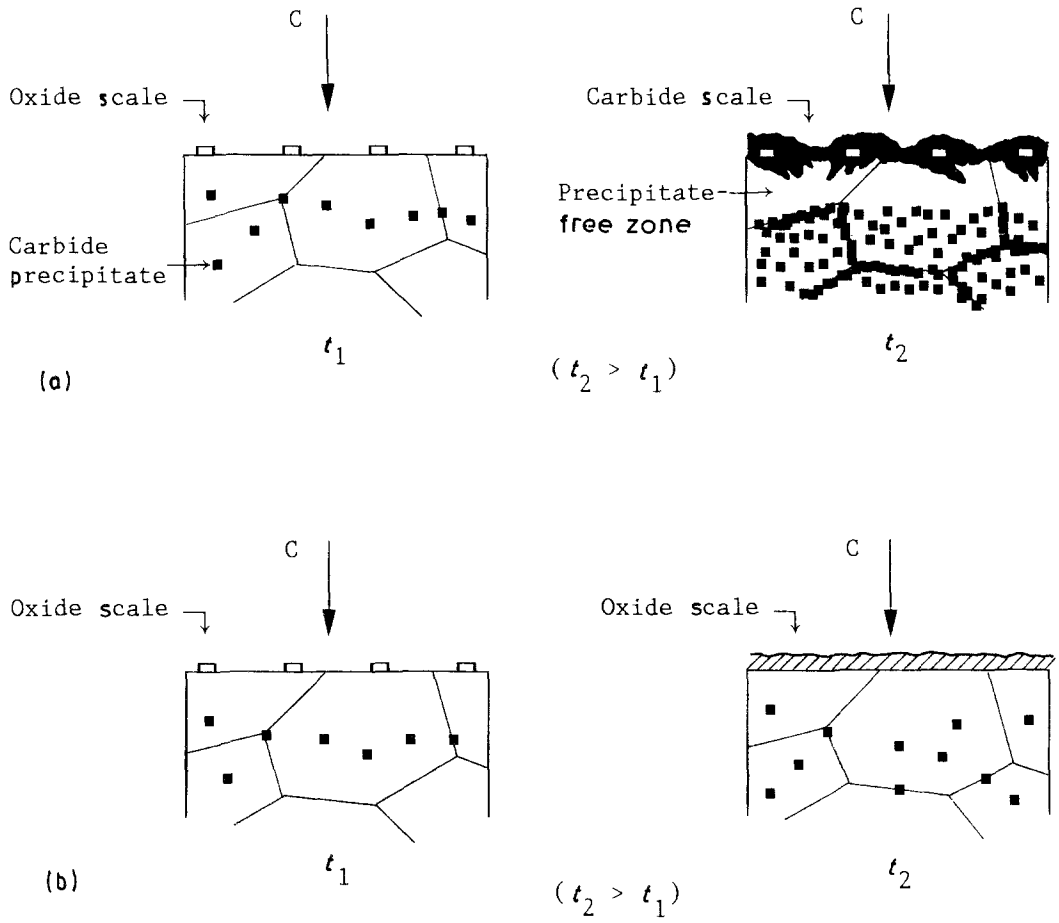

Figure 10 Schematic diagrams illustrating the progress of carburization as a function of exposure time (t) at a given temperature: (a) in the presence of a less protective surface carbide scale, (b) in the presence of a more protective surface oxide scale.

appeared to be most effective in resisting a carburization attack by acting as a barrier toward C diffusion into the alloy.

Acknowledgements

The support of the Research Institute, King Fahd University of Petroleum and Minerals and its permission to publish this work are greatly appreciated.

References

1. J. NORTON (coordinator), "Carburization in High Temperature Process Plant Materials", Colloquium Proceedings (Commission of the European Communities, BP 1003, Luxembourg, 1981).
2. J. BLACKBURN, *Mater. Perform.* **16** (12) (1977) 24.
3. G. Y. LAI, M. F. ROTHMAN and D. E. FLUCK, *Industr. Heating* (August 1985).
4. G. Y. LAI, in "High Temperature Corrosion in Energy Systems", edited by M. F. Rothman (TMS-AIME, Warrendale, Pennsylvania, 1985) p. 564.
5. G. Y. LAI and M. F. ROTHMAN, in "Corrosion 84" (National Association of Corrosion Engineers, New Orleans, Houston, Texas, 1984) Paper No. 11.
6. G. M. SMITH, D. J. YOUNG and D. L. TRIMM, *Oxid. Met.* **18** (5/6) (1982) 229.
7. J. M. HARRISON, J. F. NORTON, R. T. DERRICOTT and J. B. MARRIOTT, *Werkst. Korros.* **30** (1979) 785.
8. J. F. NORTON, L. BLIDEGEN, S. CANETOLI and P. D. FRAMPTON, *ibid.* **32** (1981) 467.
9. A. SCHNAAS and H. J. GRABKE, *Oxid. Met.* **12** (5) (1978) 387.
10. J. M. HARRISON and J. F. NORTON, in "Behavior of High Temperature Alloys in Aggressive Environments", edited by I. Kirman, J. B. Marriott, M. Merz, R. R. Sahm and D. P. Whittle (Metals Society, London, 1980) p. 661.
11. E. BULLOCK, P. D. FRAMPTON and J. F. NORTON, in "Microstructural Science", Vol. 9, edited by Gunter Petzow, R. Paris, E. D. Albrecht and J. A. McCall (Elsevier North-Holland, New York, 1981) p. 216.
12. G. H. MEIER, W. C. COONS and R. A. PERKINS, *Oxid. Met.* **18** (3/4) (1982) 235.
13. R. A. PERKINS, in "Behavior of High Temperature Alloys in Aggressive Environments", edited by I. Kirman, J. B. Marriott, M. Merz, R. R. Sahm and D. P. Whittle (Metals Society, London, 1980) p. 617.
14. O. Van der BIEST, J. M. HARRISON and J. F. NORTON, *ibid.* p. 681.
15. G. Y. LAI and R. A. JOHNSON, "Carburization of Austenitic Alloys by Gaseous Impurities in Helium", DOE Report GA-A 15790 (General Atomic Company, San Diego, CA, 1980).
16. R. B. HERCHENROEDER, G. Y. LAI and K. V. RAO, *J. Metals* **35** (11) (1983) 16.
17. H. J. GRABKE and A. SCHNASS, in "Alloy 800", edited by W. Betteridge *et al.* (North-Holland, Amsterdam, 1978) p. 195.
18. J. K. STANLEY, *J. Mater.* **5** (1970) 957.
19. K. NATESAN and T. F. KASSNER, *Met. Trans.* **4** (1973) 2557.
20. J. C. GREENBANK, *J. Iron Steel Inst.* **210** (1972) 111.
21. L. L. SHREIR, "Corrosion", 2nd Edn (Butterworths, London, 1976) p. 798.
22. J. W. EDINGTON, "Practical Electron Microscopy in Materials Science", Vol. 4 (Philips, Eindhoven, 1976) p. 33.
23. R. F. DECKER and C. T. SIMS, in "The Superalloys", edited by C. T. Sims and W. C. Hagel (Wiley, New York, 1972) p. 52.
24. A. W. SEARCY, in "Chemical and Mechanical Behavior of Inorganic Materials", edited by A. W. Searcy, D. V. Ragone and U. Columbo (Wiley-Interscience, New York, 1970) p. 33.

Received 29 October 1990
and accepted 25 March 1991